# Combining Inducible Lectin Expression and Magnetic Glyconanoparticles for the Selective Isolation of Bacteria from Mixed Populations.

Joshua E. Petch[1, 2, †], Pratik Gurnani[1], Gokhan Yilmaz[1, ‡], Francesca Mastrotto[3], Cameron Alexander[1], Stephan Heeb[2,*], Miguel Cámara [2,*] and Giuseppe Mantovani[1,*]

[1]Division of Molecular Therapeutics and Formulation, School of Pharmacy, University of Nottingham, Nottingham, NG7 2RD, UK

[2]Nottingham University Biodiscovery Institute, National Biofilms Innovation Centre, School of Life Sciences, University of Nottingham, Nottingham, NG7 2RD, UK

[3]Department of Pharmaceutical and Pharmacological Sciences, University of Padova, Via F. Marzolo 5, 35131 Padova, Italy

**ABSTRACT:** The selective isolation of bacteria from mixed populations has been investigated in varied applications ranging from differential pathogen identification in medical diagnostics and food safety to the monitoring of microbial stress dynamics in industrial bioreactors. Selective isolation techniques are generally limited to the confinement of small populations in defined locations, may be unable to target specific bacteria, or rely on upon immunomagnetic separation which is not universally applicable. In this proof-of-concept work, we describe a novel strategy combining inducible bacterial lectin expression with magnetic glyconanoparticles (MGNPs) as a platform technology to enable selective bacterial isolation from co-cultures. An inducible mutant of the Type 1 fimbriae, displaying the mannose-specific lectin FimH, was constructed in *E. coli* allowing for 'on demand' glycan-binding protein presentation following external chemical stimulation. Binding to glycopolymers was only observed upon fimbrial induction, and was specific for mannosylated materials. A library of MGNPs was produced *via* the grafting of well-defined catechol-terminal glycopolymers prepared by RAFT polymerization to magnetic nanoparticles. Thermal analysis revealed high functionalization (≥85% polymer by weight). Delivery of MGNPs to co-cultures of fluorescently labelled bacteria followed by magnetic extraction resulted in efficient depletion of Type 1 fimbriated target cells from wildtype or afimbriate *E. coli*. Extraction efficiency was found to be dependent on the molecular weight of the glycopolymers utilized to engineer the nanoparticles, with MGNPs decorated with shorter Dopa-$(ManAA)_{50}$ mannosylated glycopolymers found to perform better than those assembled from a longer Dopa-$(ManAA)_{200}$ analogue. Extraction efficiency of fimbriated *E. coli* was also improved when the counterpart strain did not harbor the genetic apparatus for expression of the Type 1 fimbriae. Overall, this work suggests that modulation of the genetic apparatus encoding bacterial surface associated lectins coupled with capture through MGNPs could be a versatile tool for the extraction of bacteria from mixed populations.

KEYWORDS: Magnetic glyconanoparticles, bacterial separation, lectins, RAFT polymerization, grafting to, microbial consortia

## INTRODUCTION

Industrial biotechnology has transformed we manufacture fine chemicals and pharmaceuticals.[1] The engineering of microbial consortia to express complex pathways in distinct modules is now enabling the production of biochemicals, such as *cis,cis*-muconic acid[2], hydroxybenzoic acid[3], biobutanol[4] and the flavonoid sakuranetin[5], at significantly higher yields than other biosynthetic production methods. Moreover, engineering metabolic modules across synthetic microbial consortia as opposed to a single chassis can reduce metabolic load upon the host organism(s) as well as limiting the crosstalk between native and non-native pathways or signalling mechanisms.[6-7]

However, the growing complexity of microbial co-cultures in bio-industrial applications will likely require specialised tools for organism differentiation, capture and processing. On-demand selective removal of bacteria from a biosynthetic fermentation culture could improve the product yield and efficiency of processing by the removal of modules which may generate non-desirable reactions.[8] This is particularly true for multi-step biosynthetic pathways split across multiple hosts, whereby depletion of a single module could push the enzymatic equilibria towards the next intermediate or the desired product.[7, 9] Furthermore, selective removal of organisms containing the desired product could aid in the mediating the shift from batch-based to continuous bioreactors further increasing synthetic yields.[10]

Several physical entrapment techniques involving microfluidics[11] and hydrogels[12], often coupled with soft lithography methods[13], have been utilised to capture bacteria in specific locations. However, these approaches are often limited to the confinement of small populations of bacterial cells in defined locations and low volumes; for microfluidic channels this is typically less than 10 μL.[14] Furthermore, physical and temporal separation lacks the ability to differentiate between phenotypically divergent cells within a population, thus limiting utility in microbial consortia.

Antibody coated magnetic nanoparticles (MNPs) have been widely used for selective bacterial isolation from

mixed populations[15], with applications ranging from detection and depletion of pathogenic organisms from foodstuffs[16] to rapid, diagnostic bioprobes.[17] Immunomagnetic capture systems have also been coupled with innovative technologies such as continuous flow microfluidics[18] or transiently magnetizable pipette tips[19] for high-throughput bacterial isolation from mixed populations at the benchtop level. However, the high cost, manufacturing issues and cold-chain requirements of immunomagnetic separation may limit the scalability of this technology. Furthermore, immunomagnetic separation techniques typically target natively expressed surface antigens on bacteria, limiting the ability to couple immunomagnetic capture to a signal.

Alternative approaches using synthetic materials have attempted to sequester bacteria with negatively-charged membranes from aqueous environments with polycations (e.g. polyethylenimine (PEI)[20], poly(allylamine hydrochloride) (PAAH)[21], poly(TMEAMA-*co*-MEDSA)[22] and poly(DMEAMA)[23]). Although synthetically scalable, these materials do not possess bacterial specificity.

In contrast, by utilizing the sugar-encoded biological language, the glycocode[24], glycomimetics may confer specificity based on the glycan preference dependent on the bacterial species.[25] Sugar-recognizing proteins, lectins, typically exhibit weak binding affinities for target monosaccharides[26]. However, lectins demonstrate high avidities and specificity for multivalent ligands, such as glycodendrimers and glycopolymers, due to the multivalent effect leading to nanomolar $K_D$ values for some synthetic glycomaterials.[27] Kiessling and co-workers utilized glycopolymers to modulate chemotactic responses in bacteria through clustering of lectin chemoreceptors,[28] while von der Ehe *et al* developed glycopolymer-cryogels as potential materials for affinity chromatography of bacterial cells.[29] We showed that modulation of glycopolymer sugar patterns can lead to preferential binding to either *S. mutans* or *E. coli*,[23] and utilized thermoresponsive polymers with pendant glucose groups to reversibly assemble/disassemble target bacteria through temperature cycling.[30] Recently, Young *et al* demonstrated that glycopolymer funtionalised gold surfaces could be used to recruit *Shewanella oneidensis* colonization and biofilm formation.[31] Furthermore, fluorescent mannose-containing glycopolymers[32] and monovalent mannose decorated magnetic nanoparticles[33] have been used as an analytic tool for the detection of fimbriated *E. coli*. To couple a stimulus to bacterial capture, Paul *et al* developed thermoresponsive mannose-functionalized p(NIPAM) microgels which could display or mask bacterial lectin ligands in a temperature dependent manner, facilitating reversible capture of *E. coli* from solution.[34]

With these developments in mind, we postulated that glycopolymer coated MNPs (MGNPs) could provide a scalable, yet selective alternative to existing materials for specific sequestration of bacterial sub-populations. Our strategy entails tightly controlled, 'on-demand' expression of lectins by bacterial sub-populations, enabling their subsequent selective sequestration and removal using appropriately sugar-encoded MGNPs. In this proof-of-principle work we first constructed an inducible mutant of the Type 1 fimbriae in *Escherichia coli,* in which the native regulatory mechanism of the *fim* operon was replaced with a regulatory system which we could control. Accordingly, chemical stimulation using anhydrotetracycline (ATc)-induced Type 1 fimbriae network expression, and our engineered strain demonstrated specific affinity for mannosylated glycomaterials due to surface expression of Type 1 fimbriae containing FimH lectin. Next, MGNPs were engineered by grafting glycopolymers to superparamagnetic iron (II,III) oxide nanoparticles (SPIONs). We showed that mannose-containing MGNPs selectively depleted Type 1 fimbriated target cells from their afimbriate counterparts in bacterial co-cultures following magnetic separation, thus highlighting the potential of this approach for selective isolation of specific bacteria form mixed populations.

## RESULTS AND DISCUSSION

### Genetic engineering of *E. coli* produces a controlled, mannosespecific binding phenotype

Initially, we genetically engineered an *E. coli* strain in which we could induce the expression of a lectin as a model system for bacterial separation. One of the best-characterized fimbrial systems identified in prokaryotes is the Type 1 fimbriae which includes the mannose-specific adhesin FimH[35], and was chosen as a model lectin in this study. FimH is displayed at the distal tip of the organelle, and includes a lectin-like domain which binds to monovalent mannose residues with $K_D$ values calculated at around 2.3 μM but has significantly higher affinities for mannose polymers and heptyl or aryl mannosides.[36]

In *E. coli* expression of the *fimAICDFGH* operon is under the control of a phase-variable regulatory circuit. Phase variation in the expression of Type 1 fimbriae is associated with the inversion of a 314-bp element, which has been dubbed the *fim* switch (*fimS*).[37] Inversion, and hence orientation, of the promoter determines the transcription levels of this operon. Furthermore, the switching of this invertible element is not dependent on RecA; it instead requires recombination by FimB or FimE. The genes encoding these regulatory recombinases are located proximally upstream of the switch. FimB and FimE specifically recognize two 9-bp inverted repeats either side of the *fim* switch.[37] FimB catalyzes the inversion of this switch in both directions at equivalent frequencies, whereas FimE catalyzes inversion at a higher frequency than FimB and only in favor of the on to off recombination.[38]

In order to eliminate the stochastic switching of the *fim* operon seen in wild type *E. coli* strains (Fig. 1A) [37] elimination of the *fim* switch and replacement with an inducible regulatory mechanism was necessary (Fig. 1B).We designed a synthetic construct containing the inducible *tetR*-$P_{tetA}$ system, a well-characterized inducible promoter with minimal leakiness and easily tunable expression levels which is activated in the presence of tetracycline or its non-bactericidal analogue anhydrotetracyline (ATc).[39] A synthetic bidirectional transcription terminator was included upstream of this promoter to minimize polar effects upstream of the chromosomal replacement. This synthetic terminator/promoter construct was flanked by regions of homology (~500 bp) to the regions of MG1655 chromosome flanking the *fimB* promoters

and the start codon of *fimA* facilitating allelic exchange with the native regulon without alteration of *fimA* sequence. A suicide plasmid derived from the R6K replicon, pDM4Cm[40], was selected as the delivery vector. The mutation cassette was cloned into this vector by standard subcloning procedures as described, yielding the plasmid pJEP1. Homology-mediated allelic exchange with pJEP1, resulted in the replacement of the native regulon of the *fim* operon with the inducible *tetR*-$p_{tetA}$ system (Fig. 1A-C).

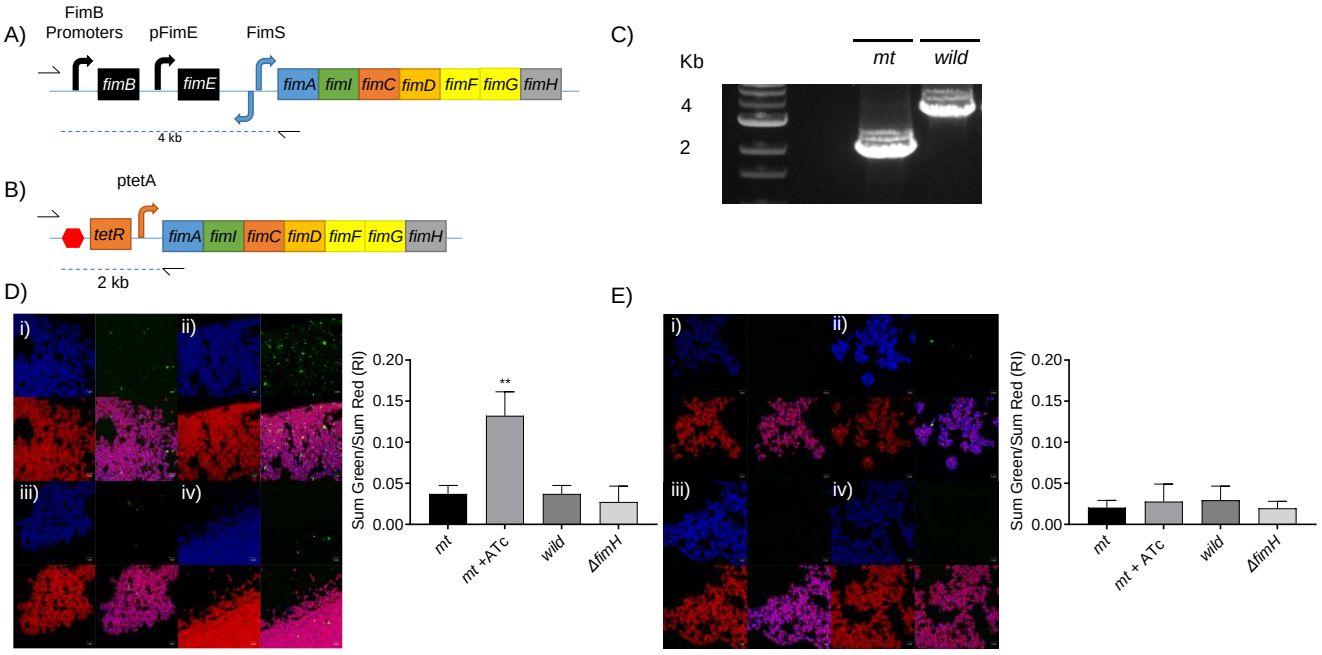


**Figure 1. Construction of an ATc inducible *tetR*-$P_{tetA}$ regulatory mutant (*mt*) of the *fim* operon in *Escherichia coli* MG1655 and phenotype confirmation by confocal microscopy. A)** schematic representation of the native *fim* operon in *E. coli* (MG1655) and associated regulatory elements. An invertible promoter element, *fimS*, regulates the downstream *fimAICDFGH* operon. Inversion is mediated by the actions of the two recombinases, FimB and FimE, which are encoded by genes upstream of the operon. **B)** Schematic representation of the *fim* operon in the regulatory mutant (*mt*), in which the native *fimS* regulatory system has been replaced by the inducible *tetR*-$P_{tetA}$ system. A synthetic bidirectional transcription terminator (red hexagon) is included upstream of *tetR*. Half arrows represent the primer pair FimF2/FimR2. **C)** PCR of mutant (*mt*) and wildtype (*wild) E. coli* (MG1655 background) with the mutation screening primer pair FimF2/FimR2, confirming chromosomal rearrangement. Representative confocal microscopy images of *E. coli* incubated with mannose- (**D**) and galactose-containing (**E**) Oregon Green-tagged glycopolymers binding. These glycopolymers were prepared and characterized in a previous work[23] and used here as fluorescent probes to confirm selective bacterial lectin binding. *E. coli* cells are stained with DAPI (blue nucleic acid dye) and FM-464fx (red membrane dye) then incubated with 10 μM poly(glycan)@Oregon Green for 1 hour to facilitate lectin mediated binding. Scale bars represent 5 μm. i) Uninduced mutant (*mt*), ii) Mutant (*mt*) induced with ATc (100ng/ml), iii) wildtype (*wild*), iv) *ΔfimH* lectin deficient knockout (JW4283-3). The relative fluorescence intensity (RI) of total polymer bound was plotted as the sum green intensity (polymer signal) divided by sum red intensity signal (membrane signal), error bars represent standard error of the mean (SEM), (n≥3 in all experiments). Analysis performed by one-way ANOVA with Tukey's Multiple Comparison Test. A significant difference in bound mannose polymer was observed between the induced mutant and all other strains (p=0.002-0.0022) but no significant difference was observed between the uninduced mutant and the other strains. No significant capture of galactose polymer was identified under any conditions.

To determine whether the replacement of the native *fim* switch in *E. coli* MG1655 with the *tetR*-$P_{tetA}$ regulatory system would result in decreased fitness of the non-native regulatory mutant, a growth assay was performed. Growth of JEP01 (the regulatory mutant), in the presence and absence of the inducer compound anhydrotetracycline (ATc) was examined in parallel with the wild type strain (MG1655) and a lectin deficient (Δ*fimH*) strain (JW4283-3). No difference in growth rate was observed under the tested conditions (Supplementary Fig. S8).

To confirm affinity of mannosylated polymers for the inducible Type 1 fimbriae mutant in the presence of the inducer, a binding assay was performed utilizing fluorescently-labelled mannosylated glycopolymers described previously by our group.[23] Glycopolymer-bacteria association was only observed in the case of the inducible Type 1 fimbriae mutant, when the medium was supplemented with ATc, a non-bactericidal inducer of the inserted *tetR*-$P_{tetA}$ regulatory apparatus (Fig. 1D). A statistically significant difference in polymer signal (sum green fluorescence intensity) divided by cell membrane signal (sum red fluorescence intensity) was observed in the case of induced mutant compared to the uninduced mutant, the wild type (MG1655) and the *ΔfimH* strains (p=0.002, 0.002 and 0.022 respectively, n≥5). These

data suggest that only the mutant, when induced by ATc, is able to bind significant quantities of mannosylated polymer and that this binding is mediated by expression of the Type 1 Fimbriae. In the absence of the inducer and, hence, absence of Type 1 fimbriae expression polymer-bacteria binding was very low (Fig. 1D). In contrast, when the same experiment was repeated with an analogous fluorescent polymer which possesses galactose pendant groups, as opposed to mannose, green fluorescence was markedly diminished (Fig 1E). In addition, the sum green fluorescence intensity over sum red fluorescence intensity for each strain, and hence the total of galactose-functional polymer bound to the bacteria as a function of cell density, was not significantly different between each strain and condition (Fig. 1E).

Taken together, these data suggest that the constructed inducible *fim* mutant was able to bind mannosylated but not galactosylated glycopolymers, which is consistent with previous reports on the binding preferences of FimH.[36, 41] This binding phenotype was exclusively displayed upon induction, suggesting tight, controllable expression of Type 1 fimbriae expression by replacement of the native regulon by the *tetR*-$P_{tetA}$ system.

### Synthesis of MGNPs by grafting dopamine terminal glycopolymers to superparamagnetic iron (II,III) oxide nanoparticles (SPIONs)

To decorate MNPs with the required glycopolymers, we followed a 'grafting to' strategy where dopamine-terminal polymers were attached to superparamagnetic iron (II,III) oxide nanoparticles (SPIONs) *via* covalent linkages between the catechol group of dopamine and the surface of SPIONs. Recent examples of similar approaches include the use of glycopolymers made by ATRP,[42] and monodisperse PEG.[43] Here, the required catechol-terminal glycopolymers were synthesized by RAFT polymerization. Accordingly, firstly a catechol-containing RAFT chain transfer agent (Dopa-PABTC, (**3**)) was synthesized, by reaction of butanethiol with carbon disulfide then with bromopropionic acid in acetone, under basic conditions. The carboxy group of the resulting intermediate was treated with *N*-hydroxysuccinimide and DCC, and the resulting activated ester was reacted with dopamine, to give the desired catechol-containing Dopa-PABTC chain transfer agent (Fig. 2A).

Then, a library of four glycopolymers were synthesized by ultrafast aqueous RAFT polymerization, which allows almost quantitative monomer conversions, while retaining good chain-end fidelity and narrow molecular weight dispersity[44]. For the synthesis of the required glycopolymers both the nature of the repeating units and the length of the polymer chains were varied. The monomers utilized were mannose (ManAA, (**5**)) and galactose (GalAA,(**7**)) acrylamides, and non-sugar control hydroxyethyl acrylamide (HEAA). Targeted degrees of polymerization (DP) were 50 and 200. $^1$H NMR analysis confirmed a good agreement between theoretical and experimental DPs of the final glycopolymers, while SEC analysis revealed narrow and monomodal molecular weight distributions and narrow dispersities ($Đ$) (Table 1, Fig. 2A). For catechol-terminal glycopolymers with $DP_{th}$ = 50, number-average molecular masses estimated by $^1$H NMR ($M_{n,NMR}$) and SEC ($M_{n,SEC}$) were in good agreement with the theoretical ones ($M_{n,th}$). for the short chain glycopolymers (Table 1). However, for control polymer Dopa-$(HEAA)_{50}$ and longer glycopolymer Dopa-$(ManAA)_{200}$ a certain deviation between $M_{n,SEC}$ and $M_{n,th}$ was observed, likely due to the difference in hydrodynamic volume between these polymers and the narrow standards used to calibrate the SEC.

The ability of these glycopolymers to selectively recognize mannose-binding lectins was then tested by surface plasmon resonance (SPR). To the best of our knowledge no methods have been reported in the literature for the immobilization of heterologously expressed bacterial FimH onto SPR sensor chips, nor is purified FimH commercially available. Thus, here Dendritic Cell-Specific Intercellular adhesion molecule-3-Grabbing Non-integrin (DC-SIGN) and mannose-binding lectin (MBL) were tested as model mannose-binding lectins. SPR results revealed that the mannose containing glycopolymers displayed a relatively strong binding avidity, with $K_D$ in the sub-nanomolar range for both lectins (Fig. 2B and 2C, and Tables S4 and S5 in the supporting information). The longer mannosylated polymer (Dopa-$(ManAA)_{200}$) demonstrated stronger binding than the shorter analogue Dopa-$(ManAA)_{50}$, potentially due to its higher glycovalency. As expected, the non-sugar polymer (Dopa-$(HEAA)_{50}$) and the non-mannose glycopolymer (Dopa-$(GalAA)_{50}$) used as negative controls did not show any specific binding to DC-SIGN and MBL. Dopa-$(ManAA)_{200}$ demonstrated the lowest $K_D$ value, thus, the highest binding avidity, for DC-SIGN (0.051 nM). Taken together, these initial experiments confirmed that Dopa-$(ManAA)_{50}$ and Dopa-$(ManAA)_{200}$ glycopolymers were able to recognize mannose-binding lectins. In principle, it is possible, or indeed likely, that other polymeric materials bearing glycans with structural similarity to mannose, for example glucose, which only differs from mannose in the stereochemistry of carbon C2 of the pyranose ring, could also bind to these model lectins and our fimbriated bacteria. However, investigation of the glycan preference and promiscuity of lectins was beyond the scope of the present work.

Next, SPIONs were synthesized by a thermal decomposition method, incorporating oleic acid for nanoparticle stabilization as described. Thermal decomposition produces small, monodisperse SPIONs of uniform shape.[43, 45] However, oleic acid-stabilized SPIONs are dispersible in relatively non-polar solvents, and only a few examples of grafting of very hydrophilic materials such as glycopolymers have been reported. Recently, Galli and co-workers displaced oleic acid on SPIONs with catechol-functionalised polyamidoamines in an aqueous system using the phase transfer catalyst tetramethylammonium hydroxide (TMAOH).[46] This method was adapted in our work here for nanoparticle decoration with catechol-terminal glycopolymers. Following exchange of oleic acid for the glycopolymers, FTIR analysis revealed a decrease of C-H stretching bands in the 2800-2900 $cm^{-1}$ consistent with the loss oleic acid (Fig. 3B). The concurrent emergence of bands at 3300 $cm^{-1}$ corresponding to the sugar O-H stretch, and at 1660 and 1550 $cm^{-1}$ for C=O stretch and N-H bend of the amido groups suggested successful decoration of the hydroxy and amido functionalities to the SPIONS consistent with catechol-terminal glycopolymer decoration.

Thermogravimetric analysis (TGA) revealed a two-step TGA profile (below 400°C) for the oleic acid capped SPIONs, similar to that described in previous studies.[43, 47] A two-step profile was also observed for Dopa-$(HEAA)_{50}$ coated nanoparticles. The final temperature at which no further weight loss is observed, around 595°C, was also similar for this material and the oleic acid capped SPIONs (Fig. 3C). This may suggest that incomplete ligand exchange was achieved between Dopa-$(HEAA)_{50}$ and oleic acid, leading to some retention of oleic acid on the particle surface. Conversely, complete vaporization of the coating material was seen by 400°C for glycopolymer-functionalized SPIONs, suggesting high replacement of oleic acid. Furthermore, TGA plots do not reveal multistep patterns for these materials, suggesting a monophasic coating of the SPION surface. Polymer weight percentage by total organic content was determined to be 89, 85, 83, and 92%, for SPION@$(HEAA)_{50}$, SPION@$(GalAA)_{50}$, SPION@$(ManAA)_{50}$ and SPION@$(ManAA)_{200}$, respectively, demonstrating high functionalization for all coatings (Fig. 3C).

Particle imaging and sizing by transmission electron microscopy (TEM) did not reveal any significant change in the diameter of the SPION core of MGNPs (~6 nm) (Fig. 3D), with the glycopolymer corona which was not clearly visible under the conditions tested. TEM also revealed that all coated nanoparticles were monodisperse and presented a consistent, spherical morphology, with no significant aggregation (Fig. 3D). MGNP size distributions were also analyzed by dynamic light scattering (DLS) (Supplementary Tables S.6, S.7 and S.8; Supplementary Figure S.12). Results (vol %) indicated that SPION@$(GalAA)_{50}$ and SPION@$(ManAA)_{50}$ had very similar size, with hydrodynamic diameter of 22.3 and 23.4 nm, respectively. This was to be expected, as the glycopolymers utilized to decorate these nanoparticles have the same chain length, and virtually identical repeating units – Gal and Man only differ for the stereochemistry at $C_2$ and $C_4$ of their pyranose ring. Conversely, SPION@$(ManAA)_{200}$ had a larger hydrodynamic diameter, 36.2 nm, which is consistent with the higher molecular weight of the glycopolymers utilized to assemble them. All MGNPs also showed a ~ 20 % (14.6-21.9 %) of larger aggregates with diameter in the 230-240 nm range.

**Table 1**. Characterisation data for catechol-terminal polymers prepared in this work.

| Polymer | $DP_{target}$ | $M_{n,th}$ (kg $mol^{-1}$)[a] | $M_{n,NMR}$ (kg $mol^{-1}$)[b] | $M_{n,SEC}$ (kg $mol^{-1}$)[c] | $Đ$[c] |
|---|---|---|---|---|---|
| Dopa-$(HEAA)_{50}$ | 50 | 6.1 | 6.3 | 10.5[d] | 1.15[d] |
| Dopa-$(GalAA)_{50}$ | 50 | 14.2 | 13.1 | 14.0 | 1.23 |
| Dopa-$(ManAA)_{50}$ | 50 | 14.2 | 16.4 | 12.8 | 1.19 |
| Dopa-$(ManAA)_{200}$ | 200 | 55.8 | 42.4 | 31.1 | 1.24 |

[a] $M_{n,th} = [([M]_0/[CTA]_0) \times \text{conversion} \times MW_{Mon}] + MW_{CTA}$. [b]Determined by $^1H$ NMR analysis. [c]Determined by SEC using aqueous 0.10 M $NaNO_3$ as the mobile phase and conventional calibration from linear PEG standards. [d]Determined by SEC, using DMF + 0.1% LiBr as the mobile phase.

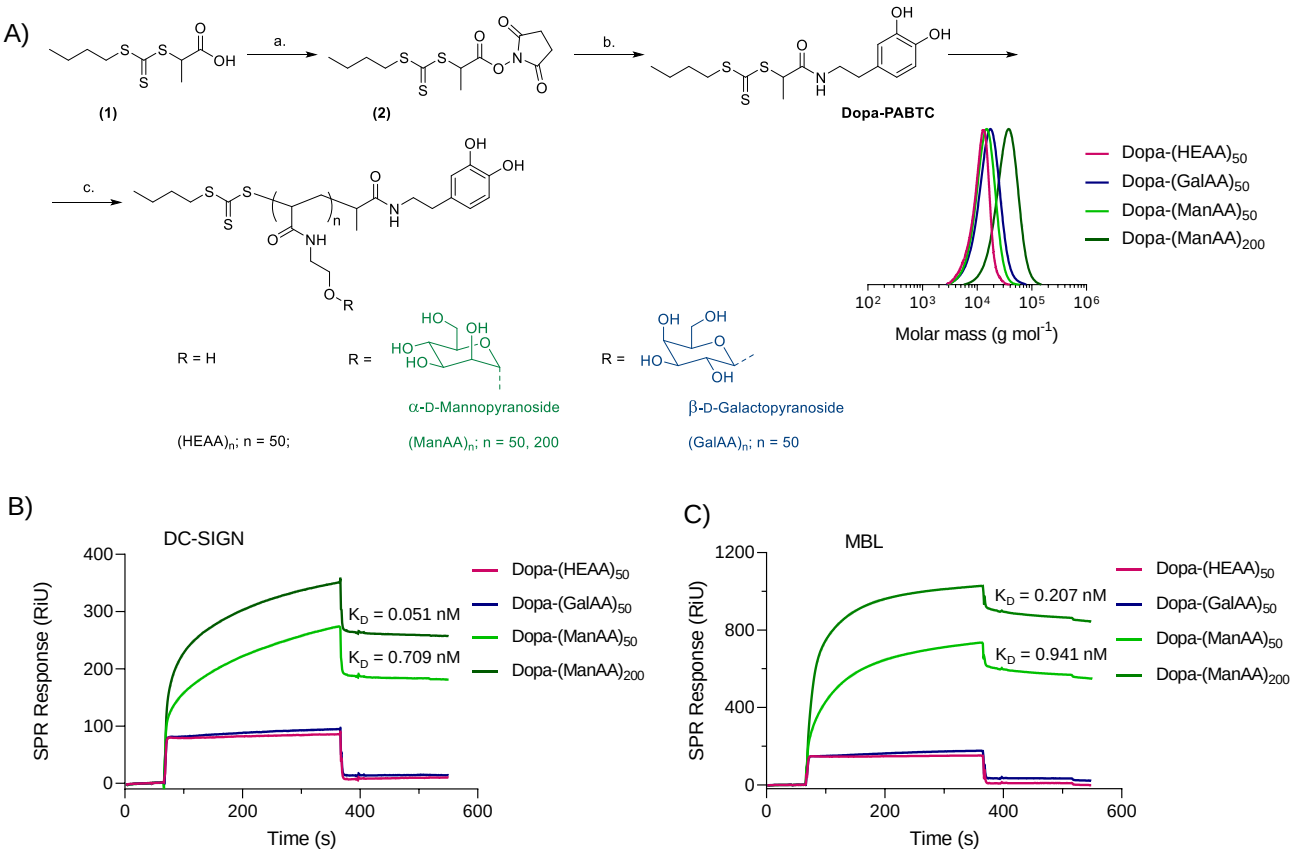


**Figure 2. Characterisation of Dopa-PABTC mediated polymers.** A) Synthesis of catechol-terminal polyacrylamides by RAFT polymerization. *Reactions and conditions*. a. *N*-hydroxysuccinimide, EDC, DMAP, $CH_2Cl_2$, 18 h, room temperature; b. dopamine hydrochloride, $Et_3N$, MeOH, 48 h, room temperature; c. 2′-acrylamidoethyl-α-D-mannopyranoside or 2′-acrylamidoethyl-α-D-galactopyranoside, VA-044, water:1,4-dioxane 4:1 vol:vol, 70°C, 2 h. SEC chromatogram traces are shown for catechol-terminal polyacrylamide polymers. B) SPR sensogram of catechol-terminal polymers with DC-SIGN at 10 nM; C) SPR sensogram of catechol-terminal polymers with MBL at 10 nM. Mannosylated polymers show association with mannose specific lectins with increasing avidity as chain length increases. HEAA and galactosylated polymers do not bind to either mannose specific lectin.

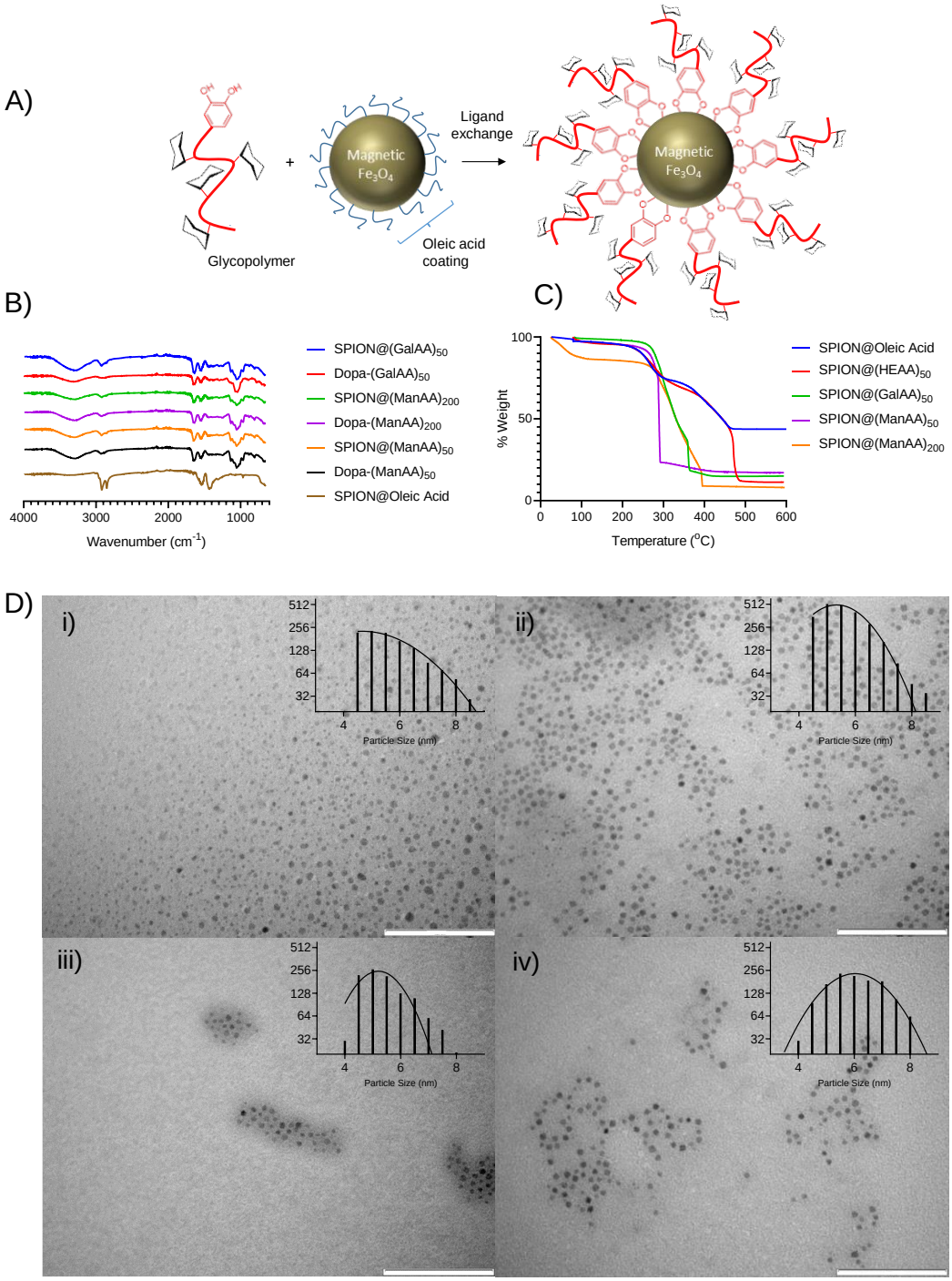


**Figure 3. Decoration of SPIONs with catechol-terminal glycopolymers.** A). Schematic representation of oleic acid ligand replacement by catechol-terminal glycopolymers. Catechol-terminal materials have a high affinity for the under-coordinated Fe surface sites of magnetic nano-particles resulting in tight binding of the bidentate ligand and replacement of the oleic acid (blue lines) producing a glycosylated iron oxide shell:core nanoparticle. B) FTIR spectra of polymer-functionalized SPIONs, compared to the corresponding free polymers, and oleic acid coated SPIONs. C) Thermal analysis of catechol-terminal polymer functionalized SPIONs. D) Representative TEM micrographs of catechol-terminal polymer functionalised SPIONs. Structure of coating material show adjacently, particle diameter distributions inset. i) SPION@Dopa-(HEAA)50 ($\bar{x}$ = 5.9 ± 1.2 nm, n= 1252, R2= 0.81; ii) SPION@Dopa-(GalAA)50 ($\bar{x}$ = 5.8 ± 1.0 nm, n= 2406, R2= 0.93. Grafting density = 1.20 chains $nm^{-2}$); iii) SPION@Dopa-(ManAA)50 ($\bar{x}$ = 5.6 ± 1.1 nm, n=1118, R2= 0.9. Grafting density = 1.00 chains $nm^{-2}$); iv) SPION@Dopa-(ManAA)200 ($\bar{x}$ = 6.1 ± 1.1 nm, n=1332, R2= 0.98. Grafting density = 0.65 chains $nm^{-2}$). Scale bars: 100 nm. Size analysis performed in ImageJ. Size distribution analysis and non-linear fit was performed in GraphPad Prism, grafting densities were calculated using the TGA grafting density equation reported by Benoit *el al* [48].

### Fluorescent labelling of target bacteria

In order to distinguish bacterial strains within a mixed population we first aimed to tag strains of interest with constitutively expressing genes coding for red and green fluorescent proteins.

The Tn7-mediated chromosomal tagging system developed by Crépin and co-workers[49] was thus modified to include expression cassettes for mRuby2[50] and eGFP under the control of the synthetic strong, insulated, constitutive promoters, $P_{11}$ and $P_{24}$.[51] By inserting these constitutive expression systems as a single copy in the chromosome, we aimed to minimize variation and noise in fluorescence data which can commonly be observed in plasmid-based expression systems due to stochastic variance in copy number between cells in a clonal population.[52]

PCR screening of the resultant transposon mutants revealed the integration of all fluorophore expression cassettes at the correct genomic locus (Supplementary Fig. S9). Growth and fluorescence analysis revealed no discernable difference in growth rates for any of the transposon mutants compared to their parental backgrounds regardless of promoter/fluorophore fusion inserted (Supplementary Figs S10 and S11). However, fluorescence cassettes under the control of the stronger promoter ($P_{24}$) uniformly demonstrated higher fluorescence outputs (Supplementary Fig. S11). Hence only $P_{24}$-controlled fluorescent protein tagged strains were taken forward for use in mixed population extraction experiments.

### Specific cellular isolation of bacteria from mixed populations mediated by MGNPs

To test the ability of the produced MGNPs to selectively isolate bacteria from a mixed population, a pulldown experiment was performed, as illustrated in Fig. 4A. An initial 1/1 co-culture of the eGFP green tagged inducible mutant and a mRuby red tagged non-target strain (wildtype or *ΔfimH*) was prepared and treated with ATc inducer to selectively promote expression of the mannose-binding Type 1 fimbriae in the eGFP green tagged mutant. The mixed culture was then incubated with MGNPs with different glycopolymer coatings, followed by magnetic extraction of SPIONs-bacteria aggregates. Spatial separation of green mannose-binding fimbriated cells from their red afimbriate neighbors was quantified by analysis of the supernatant by flow cytometry, and expressed as red:green cell ratio (Fig. 4B – Green: eGFP green tagged inducible mutant; Red: wildtype *E. coli*; Fig. 4D Green: eGFP green tagged inducible mutant; Red: lectin deficient Δ*fimH E. coli*).

Results showed successful depletion of eGFP green tagged fimbriated mutant following magnetic extraction with mannosylated MGNPs, as demonstrated by a 80.5 and 49.3% decrease for Dopa-$(ManAA)_{50}$ and Dopa-$(ManAA)_{200}$ coated nanoparticles, respectively in the mixed population containing wildtype *E. coli* cells (Fig. 4B). SPION@Dopa-$(HEAA)_{50}$ control nanoparticles were unable to deplete the green labelled inducible mutant under any conditions, confirming the interaction is glycan dependent (Fig. 4B and 4C). Some depletion of the target strain from mixed populations was also observed in the case of galactosylated materials, however this effect was both small (5% on average) and highly variable (Fig. 4B and 4C). Consequently, capture of fimbriated bacteria by galactosylated nanoparticles was statistically insignificant compared to the non-glycan decorated control, SPION@Dopa-$(HEAA)_{50}$.

Increasing mannose polymer chain length decreased isolation of the Type 1 fimbriated *E. coli*. MGNPs coated with Dopa-$(ManAA)_{50}$ were able to deplete 80.5% of the green labelled strain from the starting mixture, whereas MGNPs coated with the $DP_{200}$ mannosylated polymers only depleted 49.3% of the green labelled (Fig. 4C). Potentially, the observed difference in fimbriated *E. coli* depletion by the two mannosylated materials could be attributable to the magnetic separation step, as in Dopa-$(ManAA)_{50}$ coated MGNPs have higher proportion by weight of the magnetic iron oxide core (18%) compared to Dopa-$(ManAA)_{200}$ coated MGNPs (8%) (Fig. 3C), thus increasing the attractive magnetic force exerted on these nanoparticles. While the presence of coatings on SPIONs does not by itself appear to diminish superparamagnetic properties, some studies have shown a decrease in saturation magnetization with the presence of coating materials or increasing polymer graft densities.[53-55] Kim and co-workers suggest that coatings decrease the uniformity of SPIONs due to quenching of surface moments, thus reducing the magnetic moment of these particles[56]. It is possible that reduced magnetic saturation of Dopa-$(ManAA)_{200}$ coated SPIONs may have an effect on the efficiency of magnetic bacterial separation.

It is also possible that variance in the hydrodynamic radii of SPION@Dopa-$(ManAA)_{50}$ and SPION@Dopa-$(ManAA)_{200}$ may have some impact on the lectin interaction as this parameter could alter the spatial availability of glycan epitopes presented by nanoparticles in solution. For linear, brush and star glycopolymers those of greater size which display multiple sugar domains tend to have a higher affinity to target lectins than smaller, less valent materials, presumably due to an increase in binding epitope density[57-60]. This effect is remarkably pronounced when the size of polymers in solution matches, or exceeds, the minimum distance between binding sites on target multivalent lectins, which are typically in the order of 2-10 nm [61-62]. However, to the best of our knowledge the relationship between the hydrodynamic radius/volume of MGNPs and their affinity to target lectins has not been explored in existing literature. A decrease in grafting density was observed between SPIONs coated with glycopolymers with increasing chain length - 0.65 chains $nm^{-2}$ for SPION@Dopa-$(ManAA)_{200}$ compared to 1.00 chains $nm^{-2}$ for SPION@Dopa-$(ManAA)_{50}$ (Fig.3). Although the former MGNPs would display a larger number of mannose molecules, in principle a different arrangement of sugar epitopes on SPION@Dopa-$(ManAA)_{200}$ and SPION@Dopa-$(ManAA)_{50}$, could potentially lead to a different affinity for bacterially associated Type 1 fimbriae and contribute to the decreased extraction efficiency of Dopa-$(ManAA)_{200}$ coated MGNPs.

Intriguingly, when expression of the Type 1 fimbriae in the eGFP labelled mutant was not induced, a small proportion of the red labelled wildtype *E. coli* (MG1655::$P_{24}$mRuby) was still depleted by the MGNPs as demonstrated by a negative green depletion of 11.7 and 9.5% by Dopa-$(ManAA)_{50}$ and Dopa-$(ManAA)_{200}$ coated nanoparticles, respectively (Fig. 4B and 4C). Although depletion of the

wildtype strain could in principle be attributed to the background stochastic expression of mannose binding Type 1 fimbriae [37], leading to a small, fimbriated subpopulation which can be bound by mannosylated MGNPs, this effect is not statistically distinct to depletion of red labelled cells by the control materials, Dopa-$(HEAA)_{50}$ and Dopa-$(GalAA)_{50}$ functionalized MGNPs.

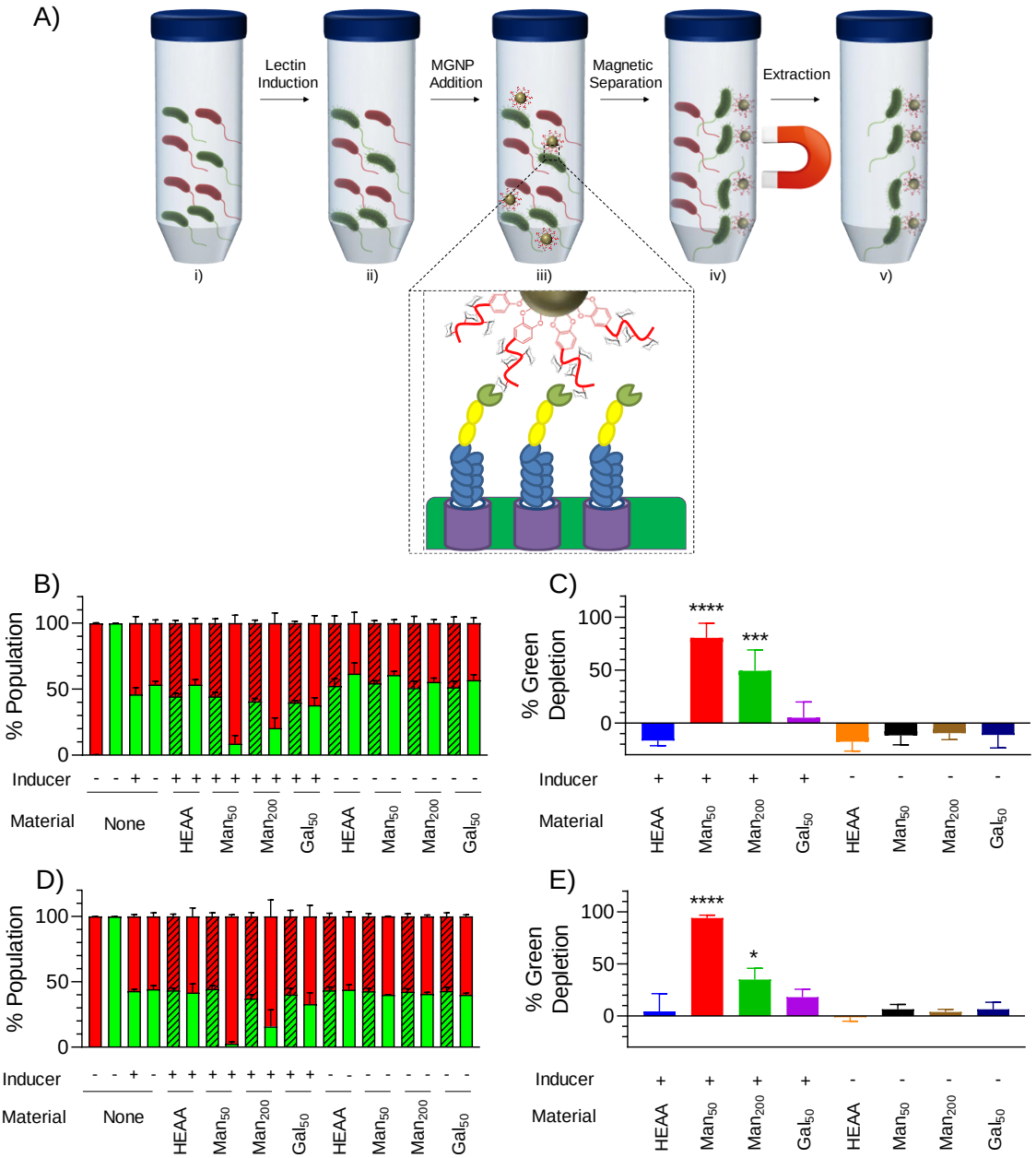


**Figure 4. Selective separation of bacteria from a mixed population facilitated by MGNPs. A)** Schematic representation of targeted bacterial depletion by MGNPs. i) Bacterial co-culture from which target isolation is desired. The target strain is genetically modified for inducible surface associated lectin expression (green), while non-target strain is lectin deficient (red). ii) Stimulus presentation facilitates cell-surface lectin expression. iii) Magnetic nanoparticles decorated with specific, macromolecular lectin ligand are added. iv) Target bacteria captured by specific MGNPs are clustered magnetically. v) Aspiration of the supernatant depletes non-target strain. **B+C)** Magnetic extraction of inducible mutant from wildtype *E. coli* by MGNPs in presence and absence of inducer. **B)** Flow cytometric analysis of mixed populations before (dashed bars) and after (smooth bars) extraction with magnetic glyconanoparticles. Green bars indicate eGFP labelled cell population percentage, red bars indicate mRuby labelled cell population percentage. **C)** Percentage depletion of eGFP labelled inducible Type 1 fimbriae mutant from mixed culture by magnetic glyconanoparticles. **D+E)** Magnetic extraction of inducible mutant from lectin deficient (*ΔfimH*) *E. coli* by MGNPs in presence and absence of inducer. **D)** Flow cytometric analysis of mixed populations before (dashed bars) and after (smooth bars) extraction with magnetic glyconanoparticles. Green bars indicate eGFP labelled cell population percentage, red bars indicate mRuby labelled cell population percentage. **C)** Percentage depletion of eGFP labelled inducible Type 1 fimbriae

mutant from mixed culture by magnetic glyconanoparticles. Poly(hydroxyethyl acrylamide) (HEAA) coated MGNPs were included as a non-sugar negative control. Data shown as mean of three independent experiments with standard deviation. **** p<0.0001; *** p=0.001; * p<0.05 compared to non-sugar material control in one-way ANOVA with Tukey's multiple comparisons test.

### Specific cellular isolation of bacteria from mixed populations by MGNPs is improved when the non-target strain is lectin deficient

In an attempt to further improve the specificity of magnetic isolation mediated by MGNPs magnetic isolation experiments were performed using an initial starting mixture of the eGFP tagged ATc-inducible Type 1 fimbriae mutant, and JW4283::$P_{24}$mRuby – the mRuby2 tagged Δ*fimH* mutant described in the first part of this manuscript.

Similar to the effect seen for the mutant/wildtype *E.coli*, extraction experiments isolation of the ATc-inducible fimbriate strain was successfully achieved with mannosylated MGNPs as demonstrated by a decrease in green fluorescent cells (Fig. 4D and 4E). SPION@Dopa-$(ManAA)_{50}$ was able to remove 94 % of the target strain from the starting mixed bacterial population, whereas MGNPs coated with Dopa-$(ManAA)_{200}$ a lower 34.8 % depletion was observed (Fig. 4E). These improved capture dynamics suggests a greater specificity of the mannosylated MGNPs to fimbriated cells when the counterpart strain does not harbor the genetic material for the expression of a lectin with competing specificity to the binding-sugar coated nanoparticles. However, a 17.9% depletion of green labelled cells was observed with SPION@Dopa-$(GalAA)_{50}$. This finding may suggest that galactosylated materials could also be capable of fimbriated cell depletion by non-specific interactions. Nevertheless, this effect is not statistically significant compared with the separation obtained with the other control nanoparticles, SPION@Dopa-$(HEAA)_{50}$, or with all materials in the absence of the inducer. This suggests that if non-specific binding is involved, its contribution to the overall binding is minimal. The higher depletion efficiency observed for the nanoparticles decorated with Dopa-$(ManAA)_{50}$ may again be attributable to a more efficient magnetic separation step, due to the higher content in iron oxide in Dopa-$(ManAA)_{50}$ compared to Dopa-$(ManAA)_{200}$, or differences in spatial availability of sugar binding units between these two MGNPs.

Additionally, in the absence of the ATc inducer, no depletion of the afimbriate strain from the starting mixed population is observed by mannosylated glyconanoparticles (Fig. 4D and 4E). Thus, lack of depletion in the absence of the inducer further supports that specificity of the magnetic isolation of fimbriated bacteria from a mixed population is improved when the counterpart strain is afimbriate.

Taken together, these results show that coupling inducible lectin expression with MGNPs mediated capture could provide a viable, highly efficient tool for bacteria isolation from a mixed population with a maximum 94% target depletion achieved under the conditions tested. Depletion of fimbriated *E. coli* was achieved with higher efficiency by MNPs coated with shorter glycopolymers and may be influenced by the sugar binding capacity of the non-target strain.

## CONCLUSIONS

In this report we have shown that bacterial subpopulations can be successfully isolated from mixed co-cultures through a strategy involving first the induction of the Type 1 fimbriae by coupling expression to an external chemical stimulus (ATc), followed by magnetic capture using SPIONs decorated with glycopolymers with specific chain length and pendant sugar ligands.

To this aim, we first constructed an inducible *fim* mutant in *E. coli* which specifically adhered to mannosylated, but not galactosylated, glycopolymers upon induction. Next, glycosylated magnetic nanoparticle were successfully engineered from SPIONs and a family of catechol-terminal glycopolymers synthesized by RAFT polymerization, through a 'grafting to' approach. Finally, the general strategy proposed in this work was demonstrated with a mixed bacterial culture containing two differentially fluorescent protein labelled *E. coli* strains which was selectively depleted of fimbriate (induced mutant) bacteria by magnetic capture using the produced MGNPs.

Isolation of fimbriated *E. coli* (*fim*$^+$) from afimbriate (*fim*$^-$) *E. coli* was near complete under the best conditions tested and isolation was most efficient when non-target strain did not harbour the genetic apparatus for expression of Type 1 fimbriae. This may suggest that genetic manipulation of target microbes may improve selectivity by MGNPs. Interestingly, in terms of initial structure-function relationship for these materials, SPION@Dopa-$(ManAA)_{50}$ proved more effective, with almost complete depletion of fimbriated *E. coli* from solution, than nanoparticles decorated with longer polymer chains, SPION@Dopa-$(ManAA)_{200}$. This was partially ascribed to a higher iron oxide content in the former, which would facilitate the magnetic extraction of target bacteria, and suggest that the efficiency of the isolation process may depend not only on the avidity by which glycopolymer ligands bind bacterial lectins, but also on the iron oxide:glycopolymer mass ratio. However, this relationship is complex and is likely also to be impacted by both the packing and orientation of glycopolymers onto the nanoparticle surface, as demonstrated by the observed difference in grafting density for MGNPs bearing different length glycopolymers, and the hydrodynamic volume of the coated MGNPs in solution.

This system complements the range of available bacterial extraction systems by utilizing materials which are synthetically scalable. Additionally, coupling varied bacterial lectin expression systems to stimulus responsive promoters could allow for 'on demand' activation of MGNP binding, leading to depletion of a target strain at a specific time or in sequential rounds as desired. It may also be possible to heterologously express non-native lectins[63] or other ligand capture proteins such as streptavidin[64] on bacterial surfaces, thus mediating their selective isolation by decorated MNPs and broaden the applications of this system further.

Finally, in principle, bacterial isolation by MGNPs may not be limited to biotechnology and could be utilized for the specific capture of bacteria from mixed populations in

a range of applications. These include replacement of immunomagnetic nanoparticles in diagnostics[65]; treatment of contaminated drinking water[66]; pathogen detection agent in the food industry[16, 67]; bioremediation[68]; extraction of biosensing strains from microbial consortia[69] and in other fundamental microbial research.

## MATERIALS AND METHODS

### Instruments and Analysis

$^{1}H$ and $^{13}C$ NMR spectra were recorded on a Bruker 400 Ultrashield spectrometer using deuterated solvents. High-resolution $^{1}H$ NMR for calculation of polymer DP was performed on a Bruker Av(III)500 spectrometer equipped with a dual $^{1}H/^{13}C$ helium-cooled cyroprobe. ESI-TOF mass spectrometry was performed on a Bruker microTOF II mass spectrometer in either HPLC grade MeCN, MeOH or milliQ $H_2O$ with a sample concentration of ≤0.01 mg/mL. Fourier Transform Infrared Spectrometry was performed on an Agilent Cary630 FTIR with an ATR module between the wavelengths of 4000-650 $cm^{-1}$ with a resolution of 2 $cm^{-1}$ with 32 background scans and 64 sample scans per sample. Thermogravimetric analysis was performed on a TA Instruments Q500 TGA in the temperature range 25-650°C with a ramp of 10 K/min under inert gas. Platinum pans were filled with ~ 5 mg of sample and the total organic content was evaluated as the mass loss fraction at 500°C by the horizontal setting.
Imaging of coated and uncoated SPIONs was performed on a Tecnai G2 transmission electron microscope (Tecnai) with an acceleration voltage of 100 kV. 13 µL of aqueous sample was deposited on a Cu200 grid with a carbon support film and negatively stained with uranyl acetate (2%) where applicable. The suspension was allowed to settle onto the grid for ~10 minutes, excess liquid removed, and the grid allowed to air dry prior to imaging. Particle sizing analysis was performed in ImageJ for >800 individual particles. Nanoparticle grafting densities were calculated using the TGA grafting density equation reported by Benoit *et al*[48]. Dynamic light scattering analysis was performed using a Malvern Zetasizer Nano-ZS at 25°C with a 4 mW He-Ne 633 nm laser at a scattering angle of 173° (back scattering). Measurements were taken assuming the refractive index (1.440) and absorption (3.0) of iron oxide. Nanoparticles were measured at 0.5 mg $mL^{-1}$ in deionised water and measured after filtration through a 0.22 µm cellulose filter in low volume (70 µL) polystyrene cuvettes. Samples were incubated for 60 seconds at 25°C prior to measurement. Measurements were repeated three times with automatic attenuation selection and measurement position. Results were analysed using Malvern DTS 6.20 software.

### Bacterial Strains and Growth Conditions.

*E. coli* strains produced and used in this work are described in Supplementary Table S1. Bacteria were grown in Lysogeny Broth (LB) liquid medium and agar plates (1.5% w/v), at 37°C. For counter-selection after biparental mating, bacteria were grown in M9 minimal media supplemented with fructose (M9F) or M9F agar plates (1.5% w/v). When needed for plasmid selection, antibiotics were added to the media at the following concentrations: Ampicillin (Amp); 25 µg/mL Chloramphenicol (Cm); 25 µg/mL Kanamycin (Km); 15 µg/mL Trimethoprim (Trim) and 20 µg/mL Tetracycline (Tet). Replicative plasmid propagation was performed in strain DH5α. For cloning and propagation of suicide vectors, containing the conditional R6K origin of replication, strains S17-1(λ*pir*) or ST18 were used.

### Plasmids, DNA Constructs, and Oligonucleotides.

The plasmids constructed and used in this study are summarized in Supplementary Table S2. Oligonucleotides were synthesized by Sigma-Aldrich and are listed in Supplementary Table S2. PCRs were performed with GoTaq Green Master Mix (Promega) for standard amplifications in screenings and with Q5 High-Fidelity DNA Polymerase (New England Biolabs) for cloning purposes. All plasmid identities were confirmed by restriction digestion and Sanger sequencing (Source Bioscience) prior to use.

### Construction of an inducible *fim* mutant in the *E. coli* background MG1655

The mutation cassette for construction of an anhydrotetracyline inducible mutant of the Fim operon was synthesised by Thermo Fischer using the GeneArt Custom Gene Synthesis service. Design of this cassette is shown in Scheme S.1. The inducible mutation cassette was amplified from the pMKFimAE by PCR using primers Fim1_Fw and Fim1_Rv, (Table. S.3) then subcloned into the suicide plasmid pDM4 by restriction cloning with XhoI and XbaI. Biparental mating was performed using 3 x $10^7$ CFU/mL of donor strain *E. coli* S17-1 carrying pJEP1 and 1 x $10^7$ CFU/mL of the recipient strain (MG1655) at 30°C on M9F agar plates for 18 h. After incubation, the mating lawn was resuspended in sterile PBS and serially diluted to $10^{-3}$, spread onto $M9F_{Cm}$ plates 30°C until individual colony growth was observed (typically 2 to 3 days) to select against the donor and screen for single crossovers. To enrich the cultures for clones having accomplished double crossover events, in which the suicide plasmid was excised, the toxic effects of the *sacB* gene on cells carrying the suicide vector was exploited. Single crossover isolates were grown overnight in no salt LB medium (NSLB) at 30°C. This culture was diluted 100-fold in fresh NSLB medium supplemented with sucrose 15% and grown overnight at 30°C twice. The cultures were then serially diluted to $10^{-6}$ and 100 µL of each serial dilution was plated onto a NSLB sucrose 15% agar plate and grown overnight at 30°C. Sucrose-resistant colonies were picked from these plates and patched onto NSLB agar, and replica-plated on NSLB sucrose 15% agar and NSLB agar supplemented with chloramphenicol 25 µg/µL. Following the isolation of several $Cm^S$, $Suc^R$ colonies which had undergone double crossover homologous recombination, PCR screening was able to confirm the presence of the desired mutation at the correct chromosomal location, with an electrophoretic profile consistent with the expected size of the insertion-deletion mutation. Furthermore, Sanger sequencing of the PCR

product isolated from mutant clones aligned with the expected sequence with full identity, confirming the chromosomal presence of the designed construct (data not shown).

### Confirmation of mutant phenotype by fluorescent glycopolymer binding assay

A 5-mL culture of the strains of interest including the *fim* inducible mutant; wild type *E coli*, MG1655; and the *ΔfimH* mutant, (JW4283-3) were grown overnight in LB media at 37 °C with agitation at 200 rpm for aeration. The following morning, 5 mL of fresh LB media was inoculated with 50 µL of the overnight culture and this procedure was repeated for all strains. The fresh cultures were grown at 37°C with agitation at 200 rpm until the mid-logarithmic growth phase (typically ~0.4-0.6 at $OD_{600}$). ATc (to 100 ng/mL) was then added to the inducible mutant culture and grown for a further 2-4 hours to induce expression of the Type 1 Fimbriae. 1 mL of each culture was then dispensed into a sterile 1.5 mL microfuge tube, pelleted by centrifugation at 5000 xg for 5 min and washed 3 times with 200 µL sterile PBS. 100 µL cells of each strain/condition was aliquoted into a fresh, sterile 1.5 mL microfuge tube and stained with 1 µL 4′,6-diamidino-2-phenylindole (DAPI). DAPI solution (1 µg/mL in PBS) for 15-60 min in order to stain the cell nuclei. The cell suspensions were pelleted by centrifugation and washed 3 times with 200 µL sterile PBS. 100 µL of each strain/condition was then stained with 1 µL of the lipophilic far red dye FM 4-64FX (1 µg/mL in DMSO) in order to stain the cell membrane. The suspensions were incubated for 30 min on a turning rack at 4°C. The cell suspensions were pelleted by centrifugation and washed 3 times with 200 µL sterile PBS.The cell pellets were then resuspended in 50 µL 1 mM Oregon Green labelled mannosylated/galactosylated polymer solution for one hour at 37 °C. The cell suspensions were pelleted by centrifugation and washed 3 times with 200°µL sterile PBS. The cell suspensions were then chilled on ice for 20 min prior to the addition of 100 µL 4% paraformaldehyde (PFA) (Sigma-Aldrich) and then incubated for 15 minutes at room temperature to fix the cells. The cell suspensions were pelleted by centrifugation and washed 3 times with 200 µL sterile PBS. The pellet was then resuspended in 20 µL FluoroGel Mounting Media (GeneTex) and a 10 µL aliquot of each strain/condition was dispensed onto a high performance coverglass (D = 0.17mm, RI = 1.5255)(Zeiss). The cover glasses containing the stained cells in mounting medium were then mounted onto a Super Premium Microscopy slide (VWR) by inversion. The slides were left to cure overnight and imaged via confocal microscopy the following day. Total green and red fluorescence was quantified in Volocity Multi-Dimensional Imaging Software (Quorum Technologies) and analyzed as total green/red fluorescence in Prism (GraphPad).

### Chromosomal tagging of bacterial strains with constitutive fluorescent protein expression cassettes by tn7 transposition

The constitutive promoters $P_{11}$ and $P_{24}$ were obtained cloned in a pBBR1 replicon vector fused to eYFP[51]. eYFP was excised from these plasmids by digestion with EcoRI and BamHI. The fluorescent proteins mRuby and eGFP were amplified by PCR from pSW002-Pc-mRuby2 and pJH257-2 respectively. These primer sets had a 5' extension on the forward primer to restore the RBS (Ribosome Binding Site) lost from the pBBR1 vector series by EcoRI/BamHI digestion. The PCR products were digested with EcoRI and BamHI and then ligated into the cut pBBR1-$P_{11}$ and pBBR1-$P_{24}$ vectors yielding the pBBR1 $P_{11}$/$P_{24}$ mRuby2/eGFP vector series. Analysis of plasmid borne cassette fluorescence revealed that strong fluorescence was only seen in the case of the two strongest promoters $P_{11}$ and $P_{24}$. Next the insulated constitutive fluorescent protein expression cassettes were amplified from the pBBR1 intermediate vectors with the $P_{xx}$F/R primer set, digested with XhoI/NsiI and ligated into pGP-Tn7-Cm digested with XhoI/NsiI yielding the vector series: pGP-Tn7-Cm-$P_{11}$mRuby; pGP-Tn7-Cm-$P_{11}$eGFP; pGP-Tn7-Cm-$P_{24}$mRuby and pGP-Tn7-Cm-$P_{24}$eGFP. Since the promoter insulation motif upstream of the promoters and fluorescent protein C-termini were identical for all the constructs, a single primer set was sufficient for all mRuby/eGFP constructs A 5' extension was included on the primer set for this amplification to restore the RBS and start/valine codon which was omitted by digestion with this enzyme set. The sequence of all the resulting plasmids was verified by Sanger sequencing prior to Tn7-mediated transposition of the constitutive fluorescent protein expression cassettes onto the *E. coli* chromosome.

### Delivery of mini-Tn7 constitutive fluorescent protein expression cassettes into desired *E. coli* recipient strains

Biparental mating was performed using 3 x $10^7$ CFU/mL of donor strain *E. coli* ST18 carrying the pGP-Tn7-Cm derivative vectors harboring the mRuby2/eGFP expression cassettes and 1 x $10^7$ CFU/mL of the recipient strains carrying the transposase-encoding vector pSTNSK at 30°C on LB agar plates for 18 h. After incubation, the mating lawn was resuspended in sterile PBS and serially diluted to $10^{-3}$, spread onto $M9F_{Cm}$ plates, incubated at 42°C for 5h and then at 37 °C for 18 h. Colonies were then screened for resistance to Cm and sensitivity to Amp and Km. Since the $Amp^R$ marker is located outside of the transposable mini-Tn7 cassette on the suicide vectors, sensitivity to Amp indicates the proper integration of the mini-Tn7 cassette at the intended chromosomal *att*Tn7 site instead of any unwanted chromosomal integration of the vector. Additionally, since the transposases are encoded on a temperature-sensitive helper plasmid, incubation at 42°C was undertaken to promote the loss of these plasmids from the recipient strains, which is verified by loss of Km resistance. Furthermore, the use of M9F Cm plates selected for the growth of the recipient strains as the S17λ*pir* donors are *thi-*, *pro-* and hence are auxotrophic for these amino acids. Chromosomal integration of the mini-Tn7 transposons at the *att*Tn7 site downstream of *glmS* within various fluorescent clones was confirmed by PCR with the *glmS*/*pstS* primer pair (Table. S.3).

### General method for aqueous RAFT mediated polymerization of acrylamide glycomonomers

The synthesis of the Dopa-PABTC CTA, 2′-acrylamidoethyl-α-D-mannopyranoside and 2′-acrylamidoethyl-β-D-galactopyranoside glycomonomers and corresponding precursors is described in the Supporting Information.
In a typical polymerization a glass vial was charged with mannose acrylamide (1.00 g, 3.61 mmol, 50 eq.), Dopa-PABTC (27 mg, 0.072 mmol, 1 eq) (from a 100 mg $mL^{-1}$ stock solution in 1,4-dioxane) and VA-044 (1.16 mg, 3.61 x $10^{-3}$ mmol, 0.05 eq.) (from a stock solution of 20 mg $mL^{-1}$ in water). A stirrer bar and a water:1,4-dioxane (4:1) mixture was added, to a total volume of 3.6 mL. The reaction vessel was sealed with a rubber septum and degassed with $N_2$ for 15 min before being immersed in a preheated oil bath at 70 °C for 2 hours. Polymers with different DP were synthesized by varying the [ManAA]:[Dopa-PABTC] ratio, with constant monomer concentration (1.0 M) and [Dopa-PABTC]:[VA-044] ratio (20:1) in all reactions.
Monomer conversion was determined by $^1$H NMR analysis in DMSO-$d_6$ of the final reaction mixture, by comparing one of the monomer vinyl peak at 6.07 ppm to the CTA $CH_3$ Z-group chain end group peak (δ =0.86 ppm), in all cases ≥97% final monomer conversion was obtained. All polymers were analyzed by SEC with aqueous 0.10 M $NaNO_3$ as the mobile phase, at 35 °C. Exemplar $^1$H spectra are shown in Fig. S20-22 in the Supporting Information. DP was calculated by comparing the integral of the catechol protons (δ 6.79, 6.56, and 6.66 ppm), each set to 1, to those of the -*CH* and -$CH_2$ signals for the polymeric backbone (δ 2.17 and 1.70 ppm, respectively).

### Synthesis of superparamagnetic iron(II,III) oxide nanoparticles (SPION)

Oleic acid stabilized magnetite ($Fe_3O_4$) nanoparticles were obtained as per the thermal decomposition method reported previously, [43] with some modification. A mixture of dioctyl ether (50 mL) and oleic acid (9.36 mL, 8.38 g, 29.7 mmol, 4 eq.,) were heated to 100°C in a two neck RB flask with constant $N_2$ bubbling. After 15 min Iron(0) pentacarbonyl (7.61 mmol, 1.49 g, 1 eq., 1 mL) was then injected rapidly into the oleic acid/dioctyl ether solution and the resulting mixture was heated to 290°C with a temperature ramp of 3 °C /min. After 1 h the nanoparticle dispersion was allowed to cool to room temperature. The nanoparticles were precipitated 3x with acetone from toluene to remove the excess of oleic acid. The average size and morphology of the isolated particles were analysed by TEM.

### Decoration of SPIONs with RAFT polymerization catechol terminal glycopolymers

Modification of the hexane soluble SPIONs stabilized with oleic acid was performed via a ligand exchange reaction with the catechol-terminal polymers by a two-step ligand exchange method adapted from Galli *et al.*[46] with some modification. In a typical reaction, a suspension of 15 mg of oleic acid-stabilized SPIONs in approximately 3 ml of hexane was dried under reduced pressure, via rotary evaporation. Subsequently aqueous solution of TMAOH (0.125 M, 20 mL) was added and the vial was sonicated for a few minutes to redisperse the SPIONs, yielding a turbid mixture. To the water-dispersed SPIONs, DOPA-poly(HEAA)$_{50}$ (39 mg, 0.1 eq to $Fe_3O_4$) was added and left stirring for 48 hours. The particles were then purified from free polymer/oleic acid by dialysis against water for 3 days in 100 kDa MWCO Spectra-Por Float-A-Lysers (Merck). The particles were then lyophilized to yield a fine black powder which responded to an external magnetic field and was easily redispersible in water. A sample of the lyophilized powder was analyzed by FTIR, TGA and TEM to confirm presence of the polymer coating, estimate the amount of polymer in polymer-SPIONs conjugates, and for size distribution analysis.

### Surface Plasmon Resonance (SPR) and kinetics

The extent of interaction between the glycopolymers and lectins were analyzed on a BIAcore 3000 system (GE Healthcare). DC-SIGN and MBL (0.025 mg/ml) were immobilized via a standard amino coupling protocol onto a CM5 sensor chip that was activated by flowing a 1:1 mixture of 0.1 M *N*-hydroxysuccinimide and 0.1 M *N*-ethyl-*N*'-(dimethylaminopropyl)carbodiimide over the chip for 6 min at 25 °C at a flow rate of 20 µL/min after system equilibration with filtered HEPES buffer (10 mM HEPES, 150 mM NaCl, 5 mM CaCl2) supplemented with 0.005% TWEEN® 20 at pH= 7.4. Subsequently, channels 1 (blank), 2, 3 and 4 were blocked by following a solution of ethanolamine (1 M pH 8.5) for 10 min at 5 µL/min to remove remaining reactive groups on the channels. Sample solutions were prepared at varying concentrations (10 nM-0.625 nM) in the same HEPES buffer to calculate the binding kinetics. Sensorgrams for each glycopolymer concentration were recorded with a 300 seconds injection of polymer solution (on period) followed by 150 seconds of buffer alone (off period). Regeneration of the sensor chip surfaces was performed using 10 mM HEPES pH 7.4, 150 mM NaCl, 10 mM EDTA, 0.01% P20 surfactant solution. Kinetic data were evaluated using a single set of sites (1:1 Langmuir Binding) model in the BIAevalulation 3.1 software

### Magnetic Isolation of target bacteria from mixed populations by magnetic glyconanoparticles (MGNPs)

A total of 5 ml cultures of each JEP01::p24eGFP and non-target controls (JW4283::p24mRuby/MG1655::p24mRuby) were grown in LB media overnight supplemented with chloramphenicol (25 µg/ml). The following morning the $OD_{600}$ of these cultures was measured and used to inoculate 5 ml of fresh LB for individual cultures and the two mixed cultures, with $OD_{600}$ normalized to 0.05. These day cultures were then incubated at 37°C for 2 hours, prior to the addition of ATc (50ng/ml), where appropriate, and further incubation for another 3 hours to induce expression of the fimbriae in one of the mixed cultures. After 5 hours of growth, 100 µL of each culture (JEP01::p24eGFP alone, JW::p24mRuby alone, mixed culture with ATc, mixed culture without ATc) were transferred into 1.5 mL Eppendorf tube. The cell pellet was collected by centrifugation and washed twice with sterile PBS. The cell pellet was then resuspended in 200 µL of nanoparticle solution for each coated nanoparticle sample (SPION@Dopa-(HEAA)$_{50}$, SPION@Dopa-(GalAA)$_{50}$, SPION@Dopa-(ManAA)$_{50}$, SPION@Dopa-(Man)$_{200}$; all at 5 mg/ml in sterile PBS) and left on a magnetic extraction rack

overnight at 4 °C. The following morning, the supernatant and pellet were recovered for each sample. Cells from were then collected by centrifugation, washed twice with sterile PBS and resuspended in 500 µL sterile PBS. The relative proportion of each strain was then estimated by flow cytometry using an Astrios EQ cell sorter (Beckman Coulter).

## ASSOCIATED CONTENT

### Supporting Information.

Further information on plasmids, bacterial strain construction, validation and additional material construction data. This material is available free of charge via the Internet at http://pubs.acs.org.

## AUTHOR INFORMATION


### Corresponding Author

*Correspondence to: Dr Giuseppe Mantovani (Email: giuseppe.mantovani@.nottingham.ac.uk), Prof Miguel Camara (miguel.camara@nottingham.ac.uk), and Dr Stephan Heeb (stephan.heeb@nottingham.ac.uk).

### Present Addresses

†Medical School, University of Nottingham, Queen's Medical Centre, Nottingham NG7 2UH, UK
‡Department of Chemistry, University of Warwick, CV4 7AL


### Author Contributions

JEP led the writing of the manuscript. JEP performed strain construction and validation experiments. FM produced fluorescently labelled glycopolymers. JEP and PG designed, synthesized and characterized MGNPs. JEP and PG synthesized Dopa-PABTC. JEP synthesized ManAA. GY and JEP synthesized GalAA. JEP and GY performed SPR experiments. JEP designed and performed magnetic pulldown experiments. GM, SH, and MC conceptualized and advised on the project, secured funding and contributed to writing of the manuscript. CA advised on, and contributed to, manuscript writing. All authors have given approval to the final version of the manuscript.

### Acknowledgments


This work was supported by the Biotechnology and Biological Sciences Research Council [grant number BB/L013940/1]. This work is affiliated with the BBSRC/EPSRC Synthetic Biology Research Centre (SBRC), University of Nottingham, through the SBRC Doctoral Training Partnership. MC is partly funded by the National Biofilms Innovation Centre (NBIC) which is an Innovation and Knowledge Centre funded by the Biotechnology and Biological Sciences Research Council, InnovateUK and Hartree Centre [grant number BB/R012415/1].

We thank Professor Charles Dozois for the kind gift of the pSTNSK and pGP-Tn7 vectors series, and Erik Hanko and Naglis Malys for their kind donation of the $P_{11}$ and $P_{24}$ promoters. Thanks are also extended to Robert Markus for his assistance in confocal microscopy experiments, Denise McLean for assistance in TEM, Rosa Catania and Gokhan Takan for aid in monomer synthesis, and Eduards Krumins for supporting TGA analysis.


## REFERENCES


(1) Singh, R. Facts, Growth, and Opportunities in Industrial Biotechnology. *Org. Process Res. Dev.* **2011,** *15* (1), 175-179
(2) Zhang, H. R.; Li, Z. J.; Pereira, B.; Stephanopoulos, G. Engineering E. coli-E. coli Cocultures for Production of Muconic Acid from Glycerol. *Microb. Cell Fact.* **2015,** *14*, 10
(3) Zhou, Y. Y.; Li, Z. H.; Wang, X. N.; Zhang, H. R. Engineering E. coli-E. coli Cocultures for Production of Muconic Acid from Glycerol. *Eng. Life Sci.* **2019,** *19* (5), 389-395
(4) Saini, M.; Chiang, C. J.; Li, S. Y.; Chao, Y. P. Production of Biobutanol from Cellulose Hydrolysate by the Escherichia coli Co-culture System. *FEMS Microbiol. Lett.* **2016,** *363* (4), 5
(5) Wang, X. N.; Li, Z. H.; Policarpio, L.; Koffas, M. A. G.; Zhang, H. R. De Novo Biosynthesis of Complex Natural Product Sakuranetin Using Modular Co-culture Engineering. *Appl. Microbiol. Biotechnol.* **2020,** *104* (11), 4849-4861
(6) McCarty, N. S.; Ledesma-Amaro, R. Synthetic Biology Tools to Engineer Microbial Communities for Biotechnology. *Trends Biotechnol.* **2019,** *37* (2), 181-197
(7) Roell, G. W.; Zha, J.; Carr, R. R.; Koffas, M. A.; Fong, S. S.; Tang, Y. J. J. Engineering microbial consortia by division of labor. *Microb. Cell Fact.* **2019,** *18*, 11
(8) Bernstein, H. C.; Brislawn, C.; Renslow, R. S.; Dana, K.; Morton, B.; Lindemann, S. R.; Song, H. S.; Atci, E.; Beyenal, H.; Fredrickson, J. K.; Jansson, J. K.; Moran, J. J. Trade-offs between Microbiome Diversity and Productivity in a Stratified Microbial *Isme J.* **2017,** *11* (2), 405-414
(9) Sgobba, E.; Wendisch, V. F. Synthetic Microbial Consortia for Small Molecule Production. *Curr. Opin. Biotechnol.* **2020,** *62*, 72-79
(10) Kopp, J.; Slouka, C.; Spadiut, O.; Herwig, C. The Rocky Road From Fed-Batch to Continuous Processing With E. coli. *Front. Bioeng. Biotechnol.* **2019,** *7*, 16
(11) Boedicker, J. Q.; Vincent, M. E.; Ismagilov, R. F. Microfluidic Confinement of Single Cells of Bacteria in Small Volumes Initiates High-Density Behavior of Quorum Sensing and Growth and Reveals Its Variability. *Angew. Chem. Int. Ed.* **2009,** *48* (32), 5908-5911
(12) Johnston, T. G.; Yuan, S. F.; Wagner, J. M.; Yi, X. N.; Saha, A.; Smith, P.; Nelson, A.; Alper, H. S. Compartmentalized Microbes and Co-cultures in Hydrogels for On-demand Bioproduction and Preservation. *Nat. Commun.* **2020,** *11* (1), 11

(13) Harper, J. C.; Brozik, S. M.; Brinker, C. J.; Kaehr, B. Biocompatible Microfabrication of 3D Isolation Chambers for Targeted Confinement of Individual Cells and Their Progeny. *Anal. Chem.* **2012,** *84* ( 21), 8985–8989
(14) Wessel, A. K.; Hmelo, L.; Parsek, M. R.; Whiteley, M. Going local: technologies for exploring bacterial microenvironments. *Nat. Rev. Microbiol.* **2013,** *11* (5), 337-348
(15) Rotariu, O.; Ogden, I. D.; MacRae, M.; Badescu, V.; Strachan, N. J. C. An Immunomagnetic Separator for Concentration of Pathogenic Micro-organisms from Large Volume Samples. *J. Magn. Magn. Mater.* **2005,** *293* (1), 589-596
(16) Lim, M. C.; Park, J. Y.; Park, K.; Ok, G.; Jang, H. J.; Choi, S. W. An Automated System for Separation and Concentration of Food-borne Pathogens Using Immunomagnetic Separation. *Food Control* **2017,** *73*, 1541-1547
(17) Kumar, V.; Nath, G.; Kotnala, R. K.; Saxena, P. S.; Srivastava, A. Biofunctional Magnetic Nanotube Probe for Recognition and Separation of Specific Bacteria from a Mixed Culture. *RSC Adv.* **2013,** *3* (34), 14634-14641
(18) Cai, G. Z.; Wang, S. Y.; Zheng, L. Y.; Lin, J. H. A Fluidic Device for Immunomagnetic Separation of Foodborne Bacteria Using Self-Assembled Magnetic Nanoparticle Chains. *Micromachines* **2018,** *9* (12), 11
(19) Oh, S.; Jung, S. H.; Seo, H.; Min, M. K.; Kim, B.; Hahn, Y. K.; Kang, J. H.; Choi, S. Magnetic Activated Cell Sorting (MACS) Pipette Tip for Immunomagnetic Bacteria Separation. *Sensors Actuat. B-Chem.* **2018,** *272*, 324-330
(20) Li, Z. M.; Ma, J. Y.; Ruan, J.; Zhuang, X. Using Positively Charged Magnetic Nanoparticles to Capture Bacteria at Ultralow Concentration. *Nanoscale Res. Lett.* **2019,** *14*, 8
(21) Xu, Y. F.; Li, C. C.; Zhu, X.; Huang, W. E.; Zhang, D. Y. Application Of Magnetic Nanoparticles In Drinking Water Purification. *Environ. Eng. Manag. J.* **2014,** *13* (8), 2023-2029
(22) Magennis, E. P.; Fernandez-Trillo, F.; Sui, C.; Spain, S. G.; Bradshaw, D. J.; Churchley, D.; Mantovani, G.; Winzer, K.; Alexander, C. Bacteria-instructed Synthesis of Polymers for Self-selective Microbial Binding and Labelling. *Nat. Mater.* **2014,** *13* (7), 748-755
(23) Magennis, E. P.; Francini, N.; Mastrotto, F.; Catania, R.; Redhead, M.; Fernandez-Trillo, F.; Bradshaw, D.; Churchley, D.; Winzer, K.; Alexander, C.; Mantovani, G. Polymers for Binding of the Gram-positive Oral Pathogen Streptococcus mutans. *PLoS One* **2017,** *12* (7), 23
(24) Longwell, S. A.; Dube, D. H. Deciphering the Bacterial Glycocode: Recent Advances in Bacterial Glycoproteomics. *Curr. Opin. Chem. Biol.* **2013,** *17* (1), 41-48
(25) Moonens, K.; Remaut, H. Evolution and structural dynamics of bacterial glycan binding adhesins. *Curr. Opin. Struct. Biol.* **2017,** *44*, 48-58
(26) Le, S. T.; Malinovska, L.; Vaskova, M.; Mezo, E.; Kelemen, V.; Borbas, A.; Hodek, P.; Wimmerova, M.; Csavas, M. Investigation of the Binding Affinity of a Broad Array of l-Fucosides with Six Fucose-Specific Lectins of Bacterial and Fungal Origin. *Molecules* **2019,** *24* (12), 17
(27) Angeli, A.; Li, M. C.; Dupin, L.; Vergoten, G.; Noel, M.; Madaoui, M.; Wang, S.; Meyer, A.; Gehin, T.; Vidal, S.; Vasseur, J. J.; Chevolot, Y.; Morvan, F. Design and Synthesis of Galactosylated Bifurcated Ligands with Nanomolar Affinity for Lectin LecA from Pseudomonas aeruginosa. *ChemBioChem* **2017,** *18* (11), 1036-1047
(28) Gestwicki, J. E.; Strong, L. E.; Kiessling, L. L. Tuning Chemotactic Responses with Synthetic Multivalent Ligands. *Chem. Biol.* **2000,** *7* (8), 583-591
(29) von der Ehe, C.; Buś, T.; Weber, C.; Stumpf, S.; Bellstedt, P.; Hartlieb, M.; Schubert, U. S.; Gottschaldt, M. Glycopolymer-Functionalized Cryogels as Catch and Release Devices for the Pre-Enrichment of Pathogens. *ACS Macro Lett.* **2016,** *5* (3), 326-331
(30) Pasparakis, G.; Cockayne, A.; Alexander, C. Control of Bacterial Aggregation by Thermoresponsive Glycopolymers. *J. Am. Chem. Soc.* **2007,** *129* (36), 11014-11015
(31) Young, T. D.; Liau, W. T.; Lee, C. K.; Mellody, M.; Wong, G. C. L.; Kasko, A. M.; Weiss, P. S. Selective Promotion of Adhesion of Shewanella oneidensis on Mannose-Decorated Glycopolymer Surfaces. *ACS Appl. Mater. Interfaces* **2020,** *12* (32), 35767-35781
(32) Xue, C.; Velayudham, S.; Johnson, S.; Saha, R.; Smith, A.; Brewer, W.; Murthy, P.; Bagley, S. T.; Liu, H. Highly Water-Soluble, Fluorescent, Conjugated Fluorene-Based Glycopolymers with Poly(ethylene glycol)-Tethered Spacers for Sensitive Detection of Escherichia coli. *Chem.-Eur. J.* **2009,** *15* (10), 2289-2295
(33) Liu, L. H.; Dietsch, H.; Schurtenberger, P.; Yan, M. D. Photoinitiated Coupling of Unmodified Monosaccharides to Iron Oxide Nanoparticles for Sensing Proteins and Bacteria. *Bioconjugate Chem.* **2009,** *20* (7), 1349-1355
(34) Paul, T. J.; Rubel, S.; Hildebrandt, M.; Strzelczyk, A. K.; Spormann, C.; Lindhorst, T. K.; Schmidt, S. Thermosensitive Display of Carbohydrate Ligands on Microgels for Switchable Binding of Proteins and Bacteria. *ACS Appl. Mater. Interfaces* **2019,** *11* (30), 26674-26683

(35) Hospenthal, M. K.; Waksman, G. The Remarkable Biomechanical Properties of the Type 1 Chaperone-Usher Pilus: A Structural and Molecular Perspective. *Microbiol. Spectr.* **2019,** *7* (1), 10
(36) Bouckaert, J.; Mackenzie, J.; de Paz, J. L.; Chipwaza, B.; Choudhury, D.; Zavialov, A.; Mannerstedt, K.; Anderson, J.; Pierard, D.; Wyns, L.; Seeberger, P. H.; Oscarson, S.; De Greve, H.; Knight, S. D. The Affinity of the FimH fimbrial Adhesin is Receptor-driven and Quasi-Independent of Escherichia coli Pathotypes. *Mol. Microbiol.* **2006,** *61* (6), 1556-1568
(37) Schwan, W. R. Regulation of fim Genes in Uropathogenic Escherichia coli. *World J. Clin. Infect. Dis.* **2011,** *1* (1), 17-25
(38) Holden, N.; Blomfield, I. C.; Uhlin, B. E.; Totsika, M.; Kulasekara, D. H.; Gally, D. L. Comparative Analysis of FimB and FimE Recombinase Activity. *Microbiology-Sgm* **2007,** *153*, 4138-4149
(39) Bertram, R.; Hillen, W. The Application of Tet Repressor in Prokaryotic Gene Regulation and Expression. *Microb. Biotechnol.* **2008,** *1* (1), 2-16
(40) Milton, D. L.; Otoole, R.; Horstedt, P.; Wolf-Watz, H. Flagellin A is Essential for the Virulence of Vibrio anguillarum. *J. Bacteriol.* **1996,** *178* (5), 1310-1319
(41) Yan, X. B.; Sivignon, A.; Yamakawa, N.; Crepet, A.; Travelet, C.; Borsali, R.; Dumych, T.; Li, Z. L.; Bilyy, R.; Deniaud, D.; Feury, E.; Barnich, N.; Darfeuille-Michaud, A.; Gouin, S. G.; Bouckaert, J.; Bernard, J. Glycopolymers as Antiadhesives of E. coil Strains Inducing Inflammatory Bowel Diseases. *Biomacromolecules* **2015,** *16* (6), 1827-1836
(42) Zhang, Q.; Nurumbetov, G.; Simula, A.; Zhu, C.; Li, M.; Wilson, P.; Kempe, K.; Yang, B.; Taob, L.; Haddleton, D. M. Synthesis of Well-defined Catechol Polymers for Surface Sunctionalization of Magnetic Nanoparticles. *Polym. Chem.* **2016,** *7*, 7002-7010
(43) Lassenberger, A.; Bixner, O.; Gruenewald, T.; Lichtenegger, H.; Zirbs, R.; Reimhult, E. Evaluation of High-Yield Purification Methods on Monodisperse PEG-Grafted Iron Oxide Nanoparticles. *Langmuir* **2016,** *32* (17), 4259-4269
(44) Gody, G.; Maschmeyer, T.; Zetterlund, P. B.; Perrier, S. Pushing the Limit of the RAFT Process: Multiblock Copolymers by One-Pot Rapid Multiple Chain Extensions at Full Monomer Conversion. *Macromolecules* **2014,** *47* (10), 3451-3460
(45) Hyeon, T.; Lee, S. S.; Park, J.; Chung, Y.; Bin Na, H. Synthesis of Highly Crystalline and Monodisperse Maghemite Nanocrystallites without a Size-selection Process. *J. Amer. Chem. Soc.* **2001,** *123* (51), 12798-12801
(46) Galli, M.; Rossotti, B.; Arosio, P.; Ferretti, A. M.; Panigati, M.; Ranucci, E.; Ferruti, P.; Salvati, A.; Maggioni, D. A New Catechol-functionalized Polyamidoamine as an Effective SPION Stabilizer. *Colloid Surf. B-Biointerfaces* **2019,** *174*, 260-269
(47) Roonasi, P.; Holmgren, A. A Fourier transform infrared (FTIR) and Thermogravimetric Analysis (TGA) Study of Oleate Adsorbed on Magnetite Nano-particle Surface. *Appl. Surf. Sci.* **2009,** *255* (11), 5891-5895
(48) Benoit, D. N.; Zhu, H. G.; Lilierose, M. H.; Verm, R. A.; Ali, N.; Morrison, A. N.; Fortner, J. D.; Ayendano, C.; Colvin, V. L. Measuring the Grafting Density of Nanoparticles in Solution by Analytical Ultracentrifugation and Total Organic Carbon Analysis. *Anal. Chem.* **2012,** *84* (21), 9238-9245
(49) Crepin, S.; Harel, J.; Dozois, C. M. Chromosomal Complementation Using Tn7 Transposon Vectors in Enterobacteriaceae. *App. Environ Microb.* **2012,** *78* (17), 6001-6008
(50) Wilton, R.; Ahrendt, A. J.; Shinde, S.; Sholto-Douglas, D. J.; Johnson, J. L.; Brennan, M. B.; Kemner, K. M. A New Suite of Plasmid Vectors for Fluorescence-Based Imaging of Root Colonizing Pseudomonads. *Front. Plant Sci.* **2018,** *8*, 15
(51) Alagesan, S.; Hanko, E. K. R.; Malys, N.; Ehsaan, M.; Winzer, K.; Minton, N. P. Functional Genetic Elements for Controlling Gene Expression in Cupriavidus necator H16. *App. Environ Microb.* **2018,** *84* (19), 17
(52) Ng, J. W.; Chatenay, D.; Robert, J. Plasmid Copy Number Noise in Monoclonal Populations of Bacteria. *Phys. Rev. E* **2010,** *81* (1), 8
(53) Lachowicz, D.; Szpak, A.; Malek-Zietek, K. E.; Kepczynski, M.; Muller, R. N.; Laurent, S.; Nowakowska, M.; Zapotoczny, S. Biocompatible and Fluorescent Superparamagnetic Iron Oxide Nanoparticles with Superior Magnetic Properties Coated with Charged Polysaccharide Derivatives. *Colloid Surf. B-Biointerfaces* **2017,** *150*, 402-407
(54) Mikhaylova, M.; Jo, Y. S.; Kim, D. K.; Bobrysheva, N.; Andersson, Y.; Eriksson, T.; Osmolowsky, M.; Semenov, V.; Muhammed, M. The Effect of Biocompatible Coating Layers on Magnetic Properties of Superparamagnetic Iron Oxide Nanoparticles. *Hyperfine Interact.* **2004,** *156* (1), 257-263
(55) Maver, U.; Bele, M.; Makovec, D.; Campelj, S.; Jamnik, J.; Gaberscek, M. Incorporation and Release of Drug into/from Superparamagnetic Iron Oxide nanoparticles. *J. Magn. Magn. Mater.* **2009,** *321* (19), 3187-3192
(56) Kim, D. K.; Mikhaylova, M.; Zhang, Y.; Muhammed, M. Protective Coating of Superparamagnetic Iron Oxide Nanoparticles. *Chem. Mat.* **2003,** *15* (8), 1617-1627
(57) de la Calle, A. C.; Gerke, C.; Chang, X. J.; Grafmuller, A.; Hartmann, L.; Schmidt, S. Multivalent

Interactions of Polyamide Based Sequence-Controlled Glycomacromolecules with Concanavalin A. *Macromol. Biosci.* **2019,** *19* (6), 9
(58) Chen, Y.; Lord, M. S.; Piloni, A.; Stenzel, M. H. Correlation between Molecular Weight and Branch Structure of Glycopolymers Stars and Their Binding to Lectins. *Macromolecules* **2015,** *48* (2), 346-357
(59) Gou, Y. Z.; Geng, J.; Richards, S. J.; Burns, J.; Becer, C. R.; Haddleton, D. M. A Detailed Study on Understanding Glycopolymer Library and Con A Interactions. *J. Polym. Sci. Pol. Chem.* **2013,** *51* (12), 2588-2597
(60) Shamout, F.; Monaco, A.; Yilmaz, G.; Becer, C. R.; Hartmann, L. Synthesis of Brush-Like Glycopolymers with Monodisperse, Sequence-Defined Side Chains and Their Interactions with Plant and Animal Lectins. *Macromol. Rapid Commun.* **2020,** *41* (1), 6
(61) Jono, K.; Nagao, M.; Oh, T.; Sonoda, S.; Hoshino, Y.; Miura, Y. Controlling the Lectin Recognition of Glycopolymers via Distance Arrangement of Sugar Blocks. *Chem. Commun.* **2018,** *54* (1), 82-85
(62) Nagao, M.; Matsubara, T.; Hoshino, Y.; Sato, T.; Miura, Y. Topological Design of Star Glycopolymers for Controlling the Interaction with the Influenza Virus. *Bioconjugate Chem.* **2019,** *30* (4), 1192-1198
(63) Martinez-Alarcon, D.; Blanco-Labra, A.; Garcia-Gasca, T. Expression of Lectins in Heterologous Systems. *Int. J. Mol. Sci.* **2018,** *19* (2), 16
(64) Heinisch, T.; Schwizer, F.; Garabedian, B.; Csibra, E.; Jeschek, M.; Vallapurackal, J.; Pinheiro, V. B.; Marliere, P.; Panke, S.; Ward, T. R. E. coli Surface Display of Streptavidin for Directed Evolution of an Allylic Deallylase. *Chem. Sci.* **2018,** *9* (24), 5383-5388
(65) Li, L. Y.; Li, Q. J.; Liao, Z. Y.; Sun, Y.; Cheng, Q. S.; Song, Y.; Song, E. Q.; Tan, W. H. Magnetism-Resolved Separation and Fluorescence Quantification for Near-Simultaneous Detection of Multiple Pathogens. *Anal. Chem.* **2018,** *90* (15), 9621-9628
(66) Bohara, R. A.; Throat, N. D.; Mulla, N. A.; Pawar, S. H. Surface-Modified Cobalt Ferrite Nanoparticles for Rapid Capture, Detection, and Removal of Pathogens: a Potential Material for Water Purification. *Appl. Biochem. Biotechnol.* **2017,** *182* (2), 598-608
(67) Zhang, Z. J.; Wang, C. X.; Zhang, L. R.; Meng, Q. T.; Zhang, Y. M.; Sun, F.; Xu, Y. D. Fast Detection of Escherichia coli in Food Using Nanoprobe and ATP Bioluminescence Technology. *Anal. Methods* **2017,** *9* (36), 5378-5387
(68) Chakraborty, R.; Hazen, T. C.; Joyner, D. C.; Kusel, K.; Singer, M. E.; Sitte, J.; Torok, T. Use of Immunomagnetic Separation for the Detection of Desulfovibrio vulgaris from Environmental Samples. *J. Microbiol. Methods* **2011,** *86* (2), 204-209
(69) Xiu, Y.; Jang, S.; Jones, J. A.; Zill, N. A.; Linhardt, R. J.; Yuan, Q. P.; Jung, G. Y.; Koffas, M. A. G. Naringenin-Responsive Riboswitch-Based Fluorescent Biosensor Module for Escherichia coli Co-Cultures. *Biotechnol. Bioeng.* **2017,** *114* (10), 2235-2244

FOR TABLE OF CONTENTS ONLY